Catalysis Science & Technology

ROYAL SOCIETY OF CHEMISTRY

COMMUNICATION

View Article Online
View Journal | View Issue

Cite this: *Catal. Sci. Technol.*, 2022, 12, 3094

Received 17th December 2021,
Accepted 23rd April 2022

DOI: 10.1039/d1cy02290c

rsc.li/catalysis

Squalene–polyethyleneimine–dynamic constitutional frameworks enhancing the enzymatic activity of carbonic anhydrase†

Dan-Dan Su,[ab] Karim Aissou,[a] Yan Zhang,[c] Virginie Gervais,[d] Sebastien Ulrich *[b] and Mihail Barboiu *[a]

Carbonic anhydrase is an essential enzyme that catalyzes the hydration/dehydration of carbon dioxide, which is highly relevant to carbon capture processes. However, its efficient encapsulation in host materials is of utmost importance for the system performance (durability, stability, and efficiency). In this paper we demonstrate that polyethyleneimine–polyethylene glycol squalene constitutional nanoparticles PEI–DCFs, synthesized *via* reversible imine/amino-carbonyl chemistry, are efficient host matrixes for bovine carbonic anhydrase (bCA) encapsulation. This system showed an impressive one-order-of-magnitude-improved catalytic proficiency (k_{cat}/K_m = 7396 M^{-1} s^{-1}) as compared to bCA alone (k_{cat}/K_m = 504 M^{-1} s^{-1}). This performance rivals the current state-of-the-art systems with equivalent amounts of the enzyme, even after heating for a prolonged period at 80 °C, translating into its direct application for enhancing carbon dioxide capture and conversion.

Introduction

The significant growth of carbon dioxide (CO_2) emissions is a serious environmental and public health issue causing atmospheric pollution and the green-house effect. Many attempts have been made using electrocatalytic reduction, photosynthesis, chemical absorption and membrane transport methods to capture and store CO_2,[1,2] but so far the high costs and energy requirements restrict their effective application.[3] On the other hand, a modern alternative rests on dynamic and adaptive materials which can be obtained by cheaper and more versatile covalent/supramolecular self-assembly processes – a proof-of-concept having already reported simultaneous CO_2 capture and metal purification.[4]

During the past decades, the use of carbonic anhydrases (CAs) for CO_2 hydration and storage has attracted attention due to its high turnover rate, its environmentally benign properties and wide sources.[5] CAs are already exploited in artificial systems for applications in CO_2 hydration/dehydration,[6,7] CO_2 hydrogenation[8] or CO_2 conversion to methanol.[9] A wide range of materials have been used for CA immobilization in order to improve its tolerance to hazardous conditions such as high temperature (up to 80–100 °C), high acidity, *etc.*, but also to maintain its efficiency when embedded in artificial matrix hosts.[10] Nanotechnology has the potential to address this problem. Indeed, multivalent binders can lead to interfacial interactions/stabilization with the enzyme while also promoting its encapsulation in nano-bioreactors or biomimetic protocells. The high surface-to-volume ratio and the controllable display of binding/reactive groups have been used in artificial[11] and CA-based catalytic nanoparticles.[12,13]

The catalytic center of CAs contains a zinc-binding pocket and a hydrophobic binding pocket. In the catalytic cycle of CA, hydroxyl ions are produced under neutral pH conditions to generate bicarbonate upon reaction with CO_2. Protons are therefore byproducts which are expelled out of the catalytic center in a rate-limiting step.[14,15] While most of the host materials developed hitherto inhibit the catalytic activity of CAs either by altering the enzyme conformation or by hindering the access of the substrates to the catalytic center, a few recent systems showed an enhancement of catalytic activity instead. This peculiar behavior is best understood by the host facilitating the proton shuttle out of the active site.[16]

[a] *Institut Européen des Membranes, Adaptive Supramolecular Nanosystems Group, University of Montpellier, ENSCM-CNRS, Place E. Bataillon CC047, Montpellier, F-34095, France. E-mail: mihail-dumitru.barboiu@umontpellier.fr*
[b] *Institut des Biomolécules Max Mousseron (IBMM), CNRS, Université de Montpellier, ENSCM, Montpellier, France. E-mail: sebastien.ulrich@cnrs.fr*
[c] *Key Laboratory of Carbohydrate Chemistry and Biotechnology, Ministry of Education, School of Pharmaceutical Sciences, Jiangnan University, 1800 Lihu Avenue, Wuxi, 214122, P.R. China*
[d] *Université Paris-Saclay, CEA, CNRS, Institute for Integrative Biology of the Cell (I2BC), 91198, Gif-sur-Yvette, France*

† Electronic supplementary information (ESI) available. See DOI: https://doi.org/10.1039/d1cy02290c

We previously reported interesting results in that direction using dynamic constitutional frameworks (DCFs) which adaptively stabilize a microenvironment through confining H-bonding or electrostatic interactions on the outer enzyme surface and play the role of multi-proton sponges, both essential for an effective catalytic activation mechanism.[17,18] In this case, CA can be activated by simple addition of building blocks in aqueous solution, which are easily and modularly self-assembled *via* reversible covalent bonds on the external enzyme surface.[19]

On the other hand, solid absorbents, made with polyethyleneimine (PEI) loaded on different porous substrates, are promising materials for carbon dioxide capture.[20] The gas absorption/transport mechanism is based on the same hydrolytic reaction as performed by CA, which may further convert CO_2 into carbamic acid and/or bicarbonate at the secondary amine sites of PEI in the presence of water. This makes PEI one of the highly performing nanomaterials for CO_2 capture from flue gas or air.

Herein, we report a novel strategy, aimed to be as simple and broadly applicable as possible relating to the encapsulation of bovine carbonic anhydrase (bCA) within a polyethyleneimine (PEI)–DCF nanoparticles with enhanced catalytic activity. This results in the production of scalable biomimetic DCF–bCA nanoparticles that remarkably outperform the classical bCA activity in solution and combine the extraordinary absorption capacity of PEI materials.[20] This study leads to a greater fundamental understanding of how CA incorporation can be optimized at the nanoscale to simultaneously stabilize and activate the overall catalytic cycles of a DCF–PEI–bCA system operated under harsh conditions, as required by industrial CO_2 capture processes. The relatively straightforward development of DCF–PEI–bCA nanoparticles is a very important and previously unreported strategy. They are operating synergistically to give enhanced catalytic turnovers, higher that those resulted from the sum of the former components that are relevant to their subsequent use in larger scale applications as absorbent materials or membranes.

Results and discussion

Design and synthesis

The preparation of DCFs was carried by self-assembly of the following components: (1) 1.3.5-benzenetrialdehyde, **BTA** as a core center, PEGylated-1,1′,2-tris-norsqualene constructed from (2) hydrophobic squalene aldehyde, **SQ-CHO** with a remarkable folded conformation in water,[21] (3) hydrophilic poly(ethylene glycol)-bis-(3-aminopropyl)-terminated (Mn ~ 1500) **PEG1500**, with a favorable solubility in water and used as an artificial biocompatible chaperone for bCA refolding and limiting aggregation[22] and (4) different polyethyleneimines–PEIs: a) branched polyethyleneimine, **bPEI800** (Mn ~ 800) (12 PEI units), b) pentaethylene-hexamine, **PEH** (5 PEI units), and c) triethylenetetramine, **TAA** (3 PEI units) used as charged H-bonding heads interacting with the bCA surface and presumed to act as catalytic multivalent proton shuttles for bCA activation (Fig. 1). **DCF–PEI**, **DCF–PEH** and **DCF–TAA** were prepared *via* the aminocarbonyl/imine reversible chemistry between (1), (2), (3) and positively-charged **bPEI800**, **PEH** and **TAA**, respectively in order to quantify their role in the enhanced catalytic effects of DCF–bCA systems at room temperature and 80 °C. The ^{1}H-NMR spectra are in accordance with the proposed structures (Fig. S1–S5†).

Binding to bCA

The binding behaviors of DCFs or PEI monomers to bCA were first evaluated by monitoring the intrinsic fluorescence emission of bCA, at its maximum of emission λ_{em} = 343 nm, following the excitation at λ_{ex} = 280 nm.[23] An obvious decrease in fluorescence emission was observed, upon addition of the DCFs (**DCF–PEI**, **DCF–PEH** and **DCF–TAA**) onto an aqueous solution of bCA (Fig. 1b and S6†). From the Stern–Volmer analysis[24] the observed Stern–Volmer constants of **DCF–PEI**, **DCF–PEH** and **DCF–TAA** with bCA were determined to be 15 052 M^{-1}, 8400 M^{-1} and 7912 M^{-1} respectively (Fig. 1c). The superiority of **DCF–PEI** compared to **DCF–PEH** and **DCF–TAA** reveals that an increasing number of cationic groups results in a more effective quenching of the fluorescence emission of bCA, which can be a result of either a quenching triggered by the DCFs or by enforced structural changes of the enzyme upon binding to the DCFs. Compared with the DCFs, monomeric **bPEI800**, **PEH** and **TAA** show two orders of magnitude weaker effects, with Stern–Volmer constants of 201 M^{-1}, 121 M^{-1} and 196 M^{-1}, respectively, demonstrating the importance of multivalent presentation of positive PEIs on DCF surfaces.

Isothermal titration calorimetry (ITC) experiments were carried out in parallel (either by titrating the enzyme with ligands or by titrating ligands with bCA) and revealed marked differences (Table 1). While **DCF–PEI**, **DCF–PEH**, and **bPEI800** were found to be similarly potent binders of bCA with association constants in a narrow range of 0.93–1.02 × 10^6 M^{-1}, notable differences in thermodynamic behavior were observed. **DCF–PEI** with its cationic superiority leads to the most pronounced enthalpic contribution compared to **DCF–PEH**. **DCF–TAA** with the smallest cationic group gives the largest entropy change including contributions of the solvent entropy and the protein conformational entropy. The difference with the above fluorescence analysis indicates that binding (measured by ITC) is not correlated with the structural changes (monitored by intrinsic fluorescence measurements) of the enzyme. Altogether, these results show that the multivalency displayed by the DCF with the largest cationic group PEI (**DCF–PEI**) triggers the most drastic structural changes in bCA, through enthalpy- and entropy-driven binding, which may affect the catalytic efficiency of the enzyme. On the other hand, **DCF–TAA** with the smallest cationic group was found to be the most potent binder, with

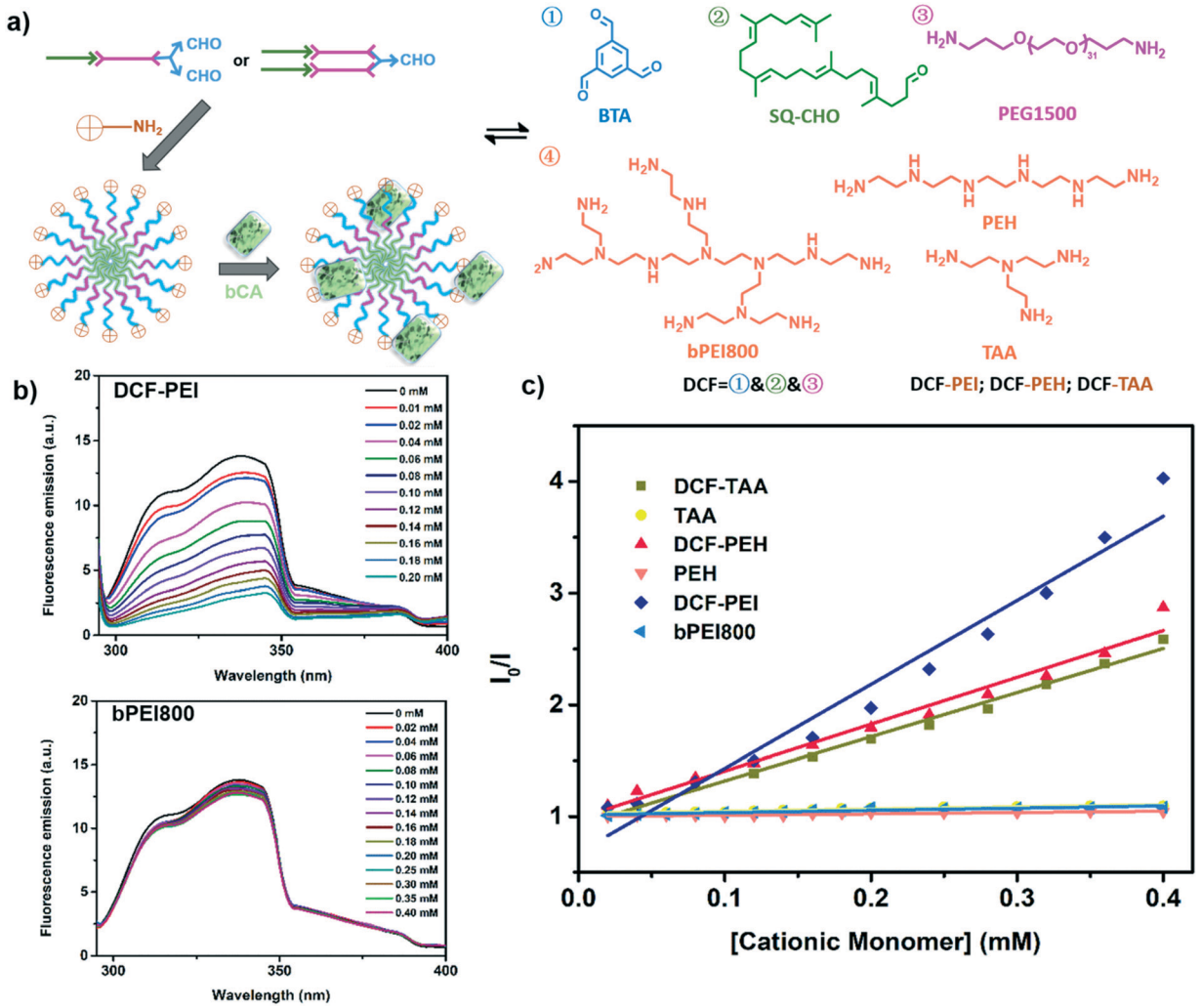

Fig. 1 a) Schematic representation of molecular components used to construct multivalent dynamic constitutional frameworks (DCFs) for bovine carbonic anhydrase (bCA) immobilization in hybrid nanoparticles. The four-component DCFs are synthesized step-wise through imine/amino-carbonyl chemistry, and different cationic headgroups (**bPEI800**, **PEH**, and **TAA**), shown in orange, were tested. b) Fluorescence spectra showing the quenching of bCA upon addition of increasing amounts of **DCF–PEI** (top) or **bPEI800** (bottom). c) Stern–Volmer plots[23] of relative fluorescence intensity *versus* cationic monomer concentration present in free and DCF bonded forms in solution, used for the determination of the Stern–Volmer constant (K_a) between bCA and DCFs/PEI monomer.

an association constant of 7.14×10^6 M^{-1} and a reaction mainly driven by entropy, but it does not trigger structural changes within the bCA enzyme according to the fluorescence assay.

Nano-scale observation of DCFs–bCA conjugates

Self-assembly at the nanoscale of DCFs–bCA conjugates. Dynamic light scattering (DLS) was used to estimate the average diameter of nanoparticles formed after 12 h at room temperature in solutions of bCA in the presence of **DCF–PEI**, **DCF–PEH** and **DCF–TAA**. First, it is worth noting that there is no fluctuation in size for the DCFs alone, within a concentration range of 0.05 mM to 0.2 mM, with average sizes of 173.5 ± 0.2 nm, 127.0 ± 0.5 nm and 171.1 ± 1.6 nm for **DCF–PEI**, **DCF–PEH** and **DCF–TAA**, respectively (Table S3†). In the presence of bCA, the DLS results showed the formation of dimensionally similar nanoparticles (Fig. 2a–c). Thus, the addition of bCA does not affect the overall self-assembly in solution, occurring with the total inclusion of enzyme within bCA/DCF nanoparticles without affecting their size and shape. In contrast, the polyamine building blocks **bPEI800**, **PEH**, and **TAA** lead to the formation of much larger

Table 1 Thermodynamic parameters derived from isothermal titration calorimetry binding studies for the binding of DCFs and PEI to bCA

Samples	K_d (μM)	K_a (10^6 M^{-1})	ΔH (kcal mol^{-1})	$-T\Delta S$ (kcal mol^{-1})
DCF–PEI	1.04 ± 0.66	0.96	−3.39 ± 0.32	−4.77
DCF–PEH	1.07 ± 0.82	0.93	−0.86 ± 0.10	−7.28
DCF–TAA	0.14 ± 0.44	7.14	−0.15 ± 0.04	−9.22
bPEI800	0.98 ± 0.84	1.02	−0.22 ± 0.04	−7.97

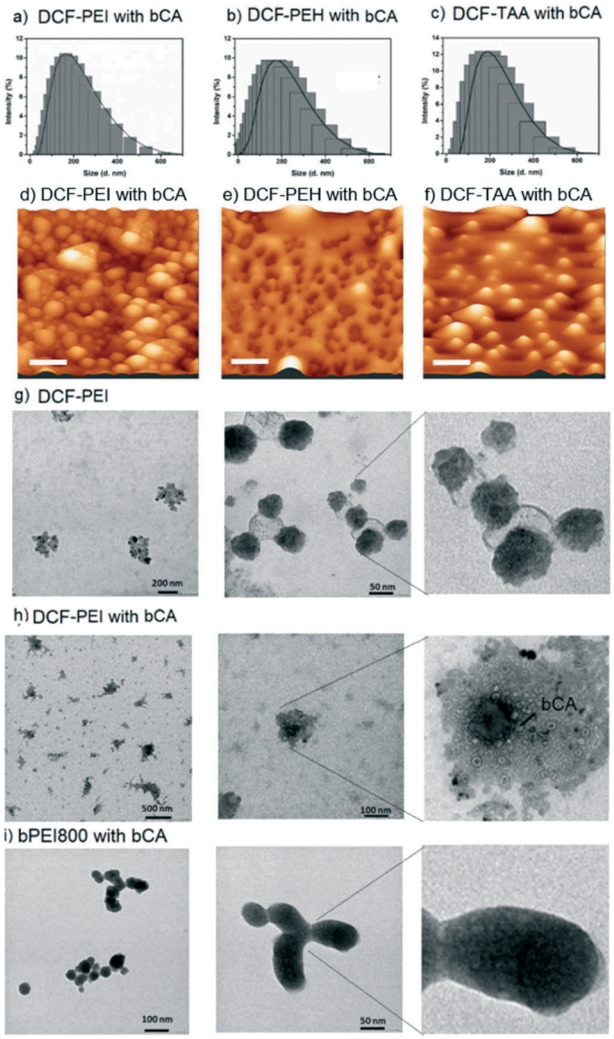

Fig. 2 DLS experiments showing the size distribution of colloidal aggregates in aqueous solutions of a) **DCF–PEI** with bCA, b) **DCF–PEH** with bCA and c) **DCF–TAA** with bCA. Representative AFM scans of d) **DCF–PEI** with bCA (1.5 × 1.5 μm; scale bar: 200 nm), e) **DCF–PEH** with bCA (1.5 × 1.5 μm; scale bar: 200 nm) and f) **DCF–TAA** with bCA (1.5 × 1.5 μm; scale bar: 200 nm). Representative TEM images of g) **DCF–PEI**, h) **DCF–PEI** with bCA and i) **bPEI800** with bCA. The dense PEI–PEG regions are darker while the less dense grey brighter spots correspond to the SQ regions. The 5 nm spots in h) correspond to the bCA dispersed in the hydrophilic corona of PEG–PEI components.

(>300 nm) and more polydisperse nanoparticles in the presence of bCA (Table S3†).

In order to further elucidate their aggregation behaviors, the bCA/DCF bioconjugates were imaged by atomic force microscopy (AFM) (Fig. 2d–f and S8†). The AFM topography images of **DCF–PEI** with bCA (Fig. 2d), **DCF–PEH** with bCA (Fig. 2e) and **DCF–TAA** with bCA (Fig. 2f) showed homogeneous particles over the entire samples, with no sign of aggregation. The apparent sizes of all samples were found to be below 200 nm, which is in good agreement with the DLS results, revealing the uniform particle distribution.

The transmission electronic microscopy TEM showed that the **DCF–PEI** (Fig. 2g) and **DCF–PEI** with bCA (Fig. 2h) had an aggregated morphology with an average overall size of 200 nm for all formulations. Similar results were obtained in previous studies on PEI decorated nanoparticles for gene delivery.[25,26] Our results are in accordance with the DLS data, confirming the narrow particle size distribution of the aggregates, which was observed by TEM. **DCF–PEI** is obtained *via* aggregation of several discrete brighter and darker nanoparticles, most probably formed by segregation of squalene and **PEG–PEI** components, respectively, self-assembled *via* reversible covalent interactions at the interfaces between nanoparticles. Interestingly **DCF–PEI** exhibited a more complex core and shell morphology when bCA is added. The aggregates were composed of a darker central core of ~50 nm and of a surrounding corona, in which well-defined and homogeneously distributed brighter nanoparticles can be identified (Fig. 2h). These white grey spots of ~5 nm are hypothesized to be mostly composed of bCA for which the crystallographic data suggest an overall ellipsoid shape with the dimensions of 4 × 4 × 5 nm.[27]

The dark color of the **bPEI800–bCA** samples suggested that strong electrostatic aggregation occurred between **bPEI800** and bCA, homogeneously distributed within dense nanoparticles. In contrast the **DCF–PEI** with the bCA sample showed that larger voids and bright less dense spots can be observed inside these hybrid samples when compared with the pristine PEI sample micrographs, where very few or no bright spots were seen.

The nano-structural distribution of dense and light regions within the **DCF–bCA** aggregates is essential to control the catalytic enzymatic performance, since they determine the pathways for the substrate flow and diffusion across the active nanoparticle.

Enzymatic activation activity of bCA

The esterase catalytic activity of cationic monomers alone/DCFs in the presence (Fig. S9†) or in the absence (Fig. S10†) of bCA was tested by monitoring the hydrolysis reaction of *p*-nitrophenyl acetate (NPA) in PBS buffer (pH 7.4) by UV-vis spectroscopy. The esterase activity through the hydrolysis reaction of NPA is directly related to CO_2 hydration reaction catalyzed by both bCA and PEI systems.[28] The time course of the absorbance at λ = 400 nm was monitored to estimate the catalytic activity relative to the reference activity of free bCA in solution at different concentrations of PEI monomers. Unless the concentration exceeds 0.1 mM, **bPEI800** and **DCF–PEI** present negligible catalytic activity in the absence of bCA (Fig. 3a), which is in line with only a few examples in the literature reporting the catalytic activity of PEI itself[28] on the CA stabilization within a PEI/dopamine protecting matrix.[29] It is also similar to the literature data where only up to 43% of the primary amine of PEI is acetylated using acetic anhydride at 60 °C in anhydrous methanol.[30] For further support, the ^{1}H NMR analysis of aqueous solutions of PEI and NPA indeed showed the exclusive formation of *p*-nitrophenol (NP) and acetic acid which completely exclude

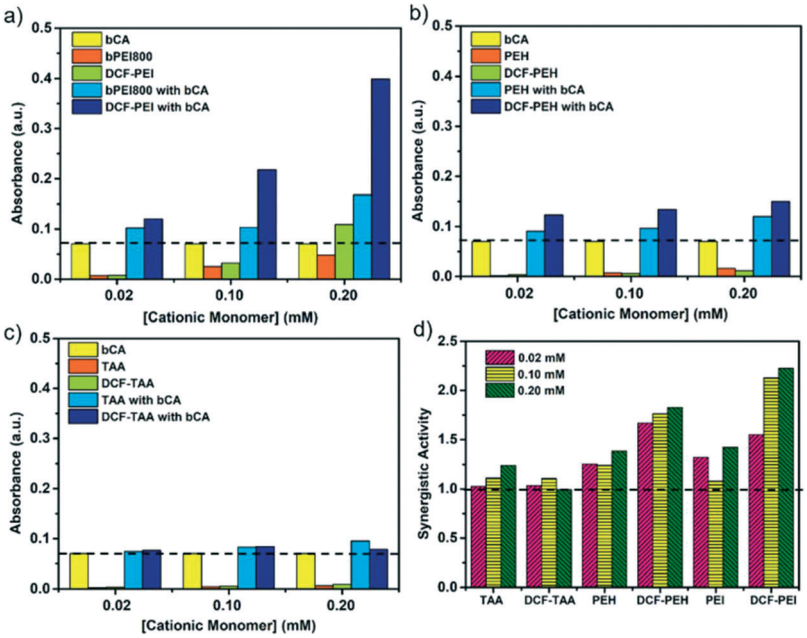

Fig. 3 Hydrolysis of *p*-NPA, monitored by UV-vis absorption spectroscopy (A – absorbance measured at 4 min) with the addition of a) **DCF–PEI**, **bPEI800**, b) **DCF–PEH**, **PEH**, c) **DCF–TAA**, **TAA** to the solutions of bCA, used as a reference. d) Synergistic activity of all monomers/DCFs.

the acetylation of PEI in aqueous solution at room temperature (Fig. S19†).

We then hypothesized that combining an increasing number of PEI with bCA in hybrid bioconjugates would lead to strong synergistic improvement of the catalytic turnover and enzyme protection within a multicharged environment. When combined with bCA, important enhancements of catalytic activity were observed for **DCF–PEI** and **bPEI800**. In the presence of bCA, the multivalent **DCF–PEI** system reaches an important ~5.8-fold increase of catalytic activity at 0.2 mM (Fig. 3a). Compared with that, **bPEI800** reached a ~2.4-fold increase in catalytic activity in the presence of bCA. In contrast, the enhancements of activity are very moderate when **PEH**, **DCF–PEH**, (Fig. 3b) and **TAA**, **DCF–TAA** (Fig. 3c) have been added to bCA, with a maximum of ~1.8-fold increase in catalytic activity observed for **DCF–PEH** at 0.2 mM of PEH.

Synergistic activity was calculated by using the following equation: $N = A_1/(A_0 + A_2)$, where A_1 is the absorbance measured with DCF or a cationic monomer with bCA at 4 min, A_0 is the absorbance measured with CA alone at 4 min, and A_2 is the absorbance measured with DCF or a monomer alone at 4 min (Fig. 3d). It is worthy to note that the synergistic activity of **DCF–PEI** and **DCF–PEH** is strongly dependent on the nature and the concentration of **bPEI800** and **PEH** monomers and shows that the multivalent effect of enzyme encapsulation by DCFs and enhanced enzyme activity play a role in the overall catalytic process.

The catalytic activity was then quantified by determining K_m, equal to the substrate concentration at half of the maximum rate V_{max}, which were both determined by fitting the data with the Michaelis–Menten model. The observed ~2-fold decrease of K_m for **DCF–PEI** with bCA (K_m = 2.08 mM) or **bPEI800** with bCA (K_m = 1.68 mM) as compared to bCA alone (K_m = 3.13 mM) reveals the stronger affinity with the bCA enzyme under DCF confinement. In contrast, **DCF–PEH**, **DCF–TAA**, **PEH**, and **TAA** show much greater K_m values (Table 2), meaning lower binding affinity which is in line with all results presented above. A proficiency constant (k_{cat}/K_m) is used to measure the catalytic efficiency of the enzymatic biohybrids. Since the proficiency constant reflects the affinity and catalytic ability of the enzyme to the substrate at the same time, it can be used to compare the catalytic efficiency of different enzymes for a specific substrate (Fig. 4a, Table 2). With k_{cat}/K_m values of 7396 and 6630 M^{-1} s^{-1} for **DCF–PEI** with bCA and **bPEI800** with bCA, respectively, these two systems clearly stand out, being one order of magnitude more powerful catalysts than all others tested, including bCA alone. It was obvious that DCF/cationic monomer with bCA presents higher catalytic efficiency, with

Table 2 The K_m values, k_{cat} values and the proficiency constant (k_{cat}/K_m) of enzymatic reaction with the addition of DCF/monomer

	K_m (mM)	k_{cat} (s^{-1})	k_{cat}/K_m (M^{-1} s^{-1})
Samples	Enzyme DCF	Enzyme DCF	Enzyme DCF
DCF–PEI	2.08	15.36	7396
DCF–PEH	4.20	3.79	902
DCF–TAA	3.71	2.49	672
Samples	Enzyme monomer	Enzyme monomer	Enzyme monomer
bPEI800	1.68	11.12	6630
PEH	3.36	2.77	826
TAA	3.31	3.24	978
bCA	3.13	1.58	504

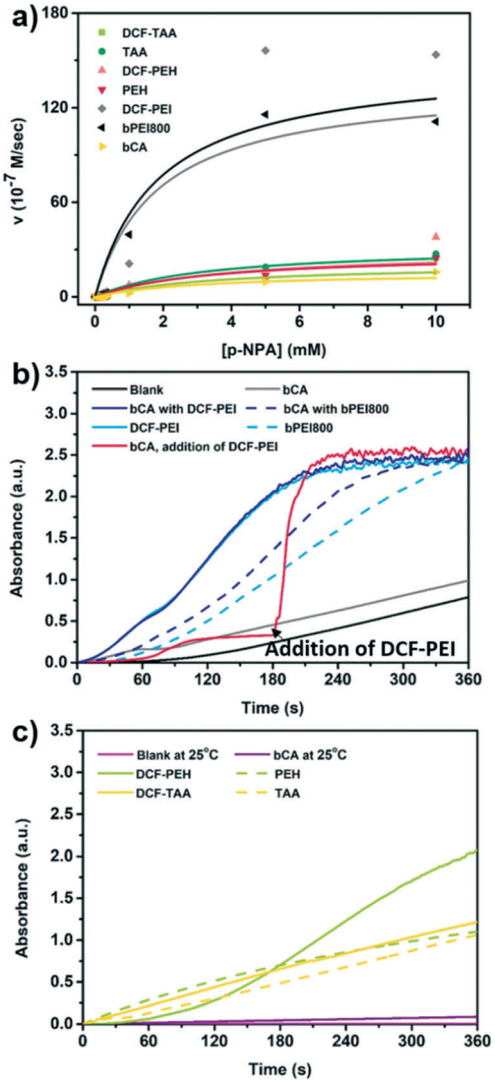

Fig. 4 Estimation of K_m of bCA enzymatic reaction based on the Michaelis–Menten equation for DCF and monomers in the a) presence of bCA. The concentration of *p*-NPA varied from 0.1 to 10 mM, and the concentration of DCFs/monomer was fixed to 0.2 mM/0.4 mM. b) and c) Kinetic hydrolysis experiments at 80 °C: blank = *p*-NPA in water at 25 °C (light magenta) and 80 °C (black), bCA at 25 °C (magenta) and 80 °C (grey); **TAA** (yellow dot), **DCF–TAA** (yellow), **PEH** (green dot), **DCF–PEH** (green), **bPEI800** (light blue dot), **DCF–PEI** (light blue) at 80 °C and bCA at 80 °C with the addition of **DCF–PEI** at 180 s (red).

an estimated k_{cat} range of 2.49 s^{-1} to 15.36 s^{-1} compared to the reaction rate k of DCF/monomer without bCA (Table S2†), emphasizing a significant catalytic effect. These results are in agreement with previous results, when the enzymatic activity of hCAII is slightly inhibited by its immobilization of PEI/polydopamine layers[31] or by the absorption on positively charged polystyrene nanoparticles that do not inhibit the enzyme.[32]

The exceptional activation effects observed with **DCF–PEI** or **bPEI800** with bCA strongly demonstrate the importance of a critical number of ethylene imine units and more importantly shed light on their multivalent presentation within DCFs. They can strongly increase the activity of bCA up to one order of magnitude under confinement within a dynamic microenvironment. Moreover, while direct interactions of monomeric PEI groups with the internal enzyme active site can lead to enzyme activation, the activation mechanism observed with nanometric hybrids is mostly related to the external binding of larger **DCF–PEI**. The multivalent network of PEI substituents mostly accelerates outwardly the proton-transfer step *via* amino groups and are equally conferring a dynamic crowding microenvironment for the enzyme activation.

The bCA aggregation driven by intermolecular hydrophobic interactions is one of the problems that hinder its use in real applications. The confinement within a protecting matrix may enhance its stability and disfavor its denaturation *via* aggregation which might occur at high temperature for example.[33,34] The activation effect of bCA at 80 °C was tested by UV experiments with the time-course analysis at pH 7.4. The final concentration of **DCF–PEI** was 0.2 mM. As shown in Fig. 4b and c, the hydrolysis reaction of *p*-nitrophenyl acetate was promoted at 25 °C (black line) as compared to the reaction with bCA at 80 °C (grey line).

Interestingly, catalytic activation effects can be obtained by simple addition of **bPEI800** (light blue dot) and **DCF–PEI** (light blue) in the absence of bCA. The addition of **bPEI800** (blue dot) and **DCF–PEI** (blue line) components to a solution of bCA induce a 3- or 5-fold, increased enzymatic activity at 80 °C, respectively. The same activation effect was observed with the addition of **DCF–PEI** in an aqueous solution of bCA after 180 s reaction time at 80 °C (red line).

The particle size of **bPEI800** with bCA and **DCF–PEI** with bCA evaluated through DLS increases to 1000–1200 nm when heated in aqueous solution at 80 °C (Fig. S16†). The same aggregation effects were observed by TEM. Heterogeneous dark and bright nanoparticles of **DCF–PEI** with bCA with an overall diameter of 800–1000 nm (Fig. S17†) are formed. Larger fractal aggregates were observed for **bPEI800** with the bCA samples when heated at 80 °C (Fig. S18†). The multivalent hydrophilic **bPEI800** and **DCF–PEI** cross-linked nanoparticles enable to activate the catalytic properties of the native bCA, through accelerated proton sponge effects of the external PEI groups. Moreover, at high temperature they strengthened significantly the structural stability, and effectively inhibited the formation of protein aggregate occurred to free bCA.

Conclusions

In conclusion, we have established that multivalent DCFs provide a possibility to enhance the bCA enzyme catalytic activity by changing the enzyme microenvironment. Moreover, those DCFs can dynamically interact and generate the optimal enzyme–DCF structure through adaptation, leading to the formation of nanoparticles that optimally encapsulate the enzyme, thereby 8-fold accelerating the

overall catalytic activity of DCF–bCA hybrids compared with bCA alone. The results obtained in this work showed that multivalent presentation of **bPEI800** groups within **DCF–PEI** platforms presents outstanding binding behaviors triggering structural changes within bCA, which results in an impressive improved catalytic proficiency of k_{cat}/K_m of 7396 M^{-1} s^{-1}, more than one order of magnitude higher than that for bCA alone. The **DCF–PEI** with bCA aggregates was notably robust and able to provide catalytic activation effects after being exposed to relatively harsh temperatures. The observations implied their feasible deployment in real systems for CO_2 capture where they would undergo cycles requiring materials to maintain high performance at 80–100 °C. This rationalization corroborates the results discussed above, suggesting that a direct perspective is to immobilize encapsulated and activated enzymes in a solid substrate for enhancing CO_2 capture and conversion. The expected performances must be greater than simple enzyme immobilization under such confined conditions within hydrophobic–hydrophilic nanoparticles. Their stability must be preserved under wet conditions, so they must be used as solid sorbents or entrapped with a high loading content in the thin layers of membranes. The "facilitated transport" with the CO_2 enzyme carriers would compensate for the low CO_2 partial pressure difference over the membrane and increase the driving force. This leads to HCO_3^- transport under wet conditions in applications where water vapors are present: flue gas, space exploration, breathing, and fermentation.[35]

Experimental

Materials and methods, Fig. S1 to S19, Tables S1 to S3, and supplementary references are provided in the ESI.†

Conflicts of interest

There are no conflicts to declare.

Acknowledgements

DS appreciates the scholarship as support from China Scholarship Council at the University of Montpellier, France. This work was supported by the M-ERA NET 2019 grant to MB *via* Agence Nationale de la Recherche ANR-20-MERA-0001-01, SMARTMATTER. YZ thanks financial support from the National Natural Science Foundation of China (NSFC) (22008090) and the Natural Science Foundation of Jiangsu Province (BK20180625). The ITC experiments were performed on the PIM Platform of I2BC (Platform for measurements of Interactions of Macromolecules).

Notes and references

1 E. E. Benson, C. P. Kubiak, A. J. Sathrum and J. M. Smieja, *Chem. Soc. Rev.*, 2009, **38**, 89–99.
2 R. Francke, B. Schille and M. Roemelt, *Chem. Rev.*, 2018, **118**, 4631–4701.
3 J. Qiao, Y. Liu, F. Hong and J. Zhang, *Chem. Soc. Rev.*, 2014, **43**, 631–675.
4 J. Septavaux, C. Tosi, P. Jame, C. Nervi, R. Gobetto and J. Leclaire, *Nat. Chem.*, 2020, **12**, 202–212.
5 J. K. J. Yong, G. W. Stevens, F. Caruso and S. E. Kentish, *J. Chem. Technol. Biotechnol.*, 2015, **90**, 3–10.
6 C. T. Supuran, *Nat. Rev. Drug Discovery*, 2008, **7**, 168–181.
7 M. Barboiu, C. T. Supuran, L. Menabuoni, A. Scozzafava, F. Mincione, F. Briganti and G. Mincione, *J. Enzyme Inhib.*, 1999, **15**, 23–46.
8 R. K. Singh, R. Singh, D. Sivakumar, S. Kondaveeti, T. Kim, J. Li, B. H. Sung, B.-K. Cho, D. R. Kim, S. C. Kim, V. C. Kaliaet, Y.-H. P. J. Zhang, H. Zhao, Y. C. Kang and J.-K. Lee, *ACS Catal.*, 2018, **8**, 11085–11093.
9 X. Ji, Z. Su, P. Wang, G. Ma and S. Zhang, *ACS Nano*, 2015, **9**, 4600–4610.
10 C. Molina-Fernández and P. Luis, *J. CO2 Util.*, 2021, **47**, 101475.
11 L. J. Prins, *Acc. Chem. Res.*, 2015, **48**, 1920–1928.
12 M. Abbas, W. P. Lipiński, J. Wang and E. Spruijt, *Chem. Soc. Rev.*, 2021, **50**, 3690–3705.
13 S. Huang, X. Kou, J. Shen, G. Chen and G. Ouyang, *Angew. Chem., Int. Ed.*, 2020, **59**, 8786–8798.
14 C. T. Supuran, *Expert Opin. Drug Metab. Toxicol.*, 2016, **12**, 423–431.
15 C. T. Supuran, *Expert Opin. Drug Discovery*, 2017, **12**, 61–88.
16 D.-D. Su, Y. Zhang, S. Ulrich and M. Barboiu, *ChemPlusChem*, 2021, **86**, 1500–1510.
17 Y. Zhang, M. Barboiu, O. Ramström and J.-H. Chen, *ACS Catal.*, 2019, **10**, 1423–1427.
18 Y. Zhang, W.-X. Feng, Y.-M. Legrand, C. T. Supuran, C.-Y. Su and M. Barboiu, *Chem. Commun.*, 2016, **52**, 13768–13770.
19 Y. Zhang, Y. C. Qi, S. Ulrich, M. Barboiu and O. Ramström, *Mater. Chem. Front.*, 2020, **4**, 489–506.
20 X. Shen, H. Du, R. H. Mullins and R. R. Kommalapati, *Energy Technol.*, 2017, **5**, 822–833.
21 D. Desmaële, R. Gref and P. Couvreur, *J. Controlled Release*, 2012, **161**, 609–618.
22 J. L. Cleland, C. Hedgepeth and D. I. Wang, *J. Biol. Chem.*, 1992, **267**, 13327–13334.
23 Y. Chen and D. M. Barkley, *Biochemistry*, 1998, **37**, 9976–9982.
24 N. J. B. Green, S. M. Pimblott and M. Tachiya, *J. Phys. Chem.*, 1993, **97**, 196–202.
25 S. S. Rohiwal, N. Dvorakova, J. Klima, M. Vaskovicova, F. Senigl, M. Slouf, E. Pavlova, P. Stepanek, D. Babuka, H. Benes, Z. Ellederova and K. Stieger, *Sci. Rep.*, 2020, **10**, 4619.
26 T.-H. Tran, S. Krishnan and M. M. Amiji, *PLoS One*, 2016, **11**, e0152024.
27 C. L. Lomelino, J. T. Andring and R. McKenna, *Int. J. Med. Chem.*, 2018, 9419521.
28 L. Y. Zakharova, A. B. Mirgorodskaya, E. I. Yackevich, A. V. Yurina, V. V. Syakaev, S. K. Latypov and A. I. Konovalov, *J. Chem. Eng. Data*, 2010, **55**, 5848–5855.
29 S. M. Gould and D. S. Tawfik, *Biochemistry*, 2005, **44**, 5444–5452.
30 N. P. Gabrielson and D. W. Pack, *Biomacromolecules*, 2006, **7**, 2427–2435.

31 J. Sun, C. Wang, Y. Wang, S. Ji and W. Liu, *J. Appl. Polym. Sci.*, 2019, **136**, 47784.
32 A. Assarsson, I. Pastoriza-Santos and C. Cabaleiro-Lago, *Langmuir*, 2014, **30**, 9448–9456.
33 M. Yan, Z. Liu, D. Lu and Z. Liu, *Biomacromolecules*, 2007, **8**, 560–565.
34 M. Y. M. Abdelrahim, C. F. Martins, L. A. Neves, C. Capasso, C. T. Supuran, I. M. Coelhoso, J. G. Crespo and M. Barboiu, *J. Membr. Sci.*, 2017, **528**, 225–230.
35 M. Sandru, S. H. Haukebo and M. B. Hagg, Composite hollow fiber membranes for CO2 capture, *J. Membr. Sci.*, 2010, **346**, 172–186.